Simulation of particle capture in a microfiltration membrane

Q. Derekx, P. Bacchin, D. Veyret, K. Glucina and P. Moulin

ABSTRACT

The present study takes an interest in the description of the fouling mechanisms by a numerical approach at the microscopic scale. At first, an X-ray tomography has enabled the modelling of the membrane structure for the numerical simulations. Next, for different particle size, a same volume of particles has been sent in the modelled membrane and the final permeability has been computed. Thus, the influence of the particle size on the fouling has been seen. An observation of the particles penetration in the membrane has been realised to detail this influence. The Hermia relations were used in order to determinate the predominant fouling mechanism or the succession of predominant fouling mechanisms. But, without an accurate calculation of the first derivative, it is not possible to define cleanly the predominant fouling mechanism for a low filtered volume. Nevertheless, the perspectives of the local approach with the numerical simulation seem interesting.

Key words | fouling, microfiltration, microscopic scale, numerical simulation, pore blocking

Q. Derekx (corresponding author)
P. Bacchin
Laboratoire de Génie Chimique (CNRS – UMR 5503),
Université Paul Sabatier,
118, route de Narbonne 31062,
Toulouse Cedex 9,
France
E-mail: *derekx@chimie.ups-tlse.fr*

P. Moulin
Laboratoire de Mécanique,
Modélisation et Procédés Propres
(CNRS – UMR 6181),
Europôle de l'Arbois,
BP 80, Bâtiment Laënnec,
Hall C 13545 Aix-en-Provence Cedex 04,
France

D. Veyret
European Commission, Joint Research Centre,
Institute of Energy,
Post Office Box 2, NL-1755ZG Petten,
The Nederlands

Q. Derekx
K. Glucina
Suez Environnement,
CIRSEE, Pôle Eau Potable,
38, rue du président Wilson 78230 Le Pecq,
France

INTRODUCTION

The fouling phenomena are always the main problem to be faced when using membrane separation in water treatment. Therefore, it is necessary to understand these phenomena to improve the control of the processes. Some global models such as the gel-polarization model or the osmotic-pressure model have already been developed, but do not well describe the complex interplay between physicochemical properties, mass transfer and hydrodynamics. These interactions occur at a microscopic scale where the membrane and the dispersion exhibit complex properties. A way to understand these phenomena is to describe the different mechanisms of fouling: complete pore blocking (a), standard pore blocking (b), intermediate pore blocking (c), and cake filtration (d) (cf. Figure 1).

The first approach was theoretical. Hermans & Bredée (1936), then Gonsalves (1950) have developed blocking filtration laws. Hermia (1982) reworked them in order to allow the distinction between the different mechanisms with only one expression. For a filtration at constant flux, the law is:

$$\frac{d\Delta P}{dV} = k(\Delta P)^i \quad (1)$$

In this expression, ΔP is the transmembrane pressure, V the filtered volume and i is the blocking index corresponding to a mechanism (Table 1).

Hermia has also extended their application for the power-law non Newtonian fluids. The studies of Grace (1956) with this approach highlight the presence of standard pore blocking for each used filter. Some experiments were realised by Bowen *et al.* (1995) and Hwang *et al.* (2008) and show there is a succession of predominant mechanisms conclude by the cake filtration. Wang & Tarabara (2008) and Seminario *et al.* (2002) have associated this approach with SEM visualisation of the membrane surface. The relative importance of each mechanism has been determined according to the particle size, the pore size and the surface density of pores. A few

doi: 10.2166/wst.2011.349

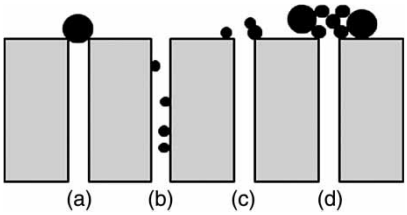

Figure 1 | Schema of the different fouling mechanisms.

Table 1 | Value of the blocking index for each mechanism

	Complete pore blocking	Standard pore blocking	Intermediate pore blocking	Cake filtration
Blocking index i	2	1.5	1	0

numerical simulations describe this succession of fouling mechanisms. Based on a random packing of spheres, Kawakatsu *et al.* (1995) developed a model for deposition of spherical particles on the membrane surface. Frey & Schmitz (2000) allows also in his model a capture in the porous media, but the geometry of the membrane is modelled as a succession of parallel channels. The aim of the present work is to pursue the description of the different fouling mechanisms by integrating the complexity of the membrane structure in the numerical simulation.

METHODS

Numerical model

The simulations were realised with the software GeoDict (Fraunhofer ITWM). The created volume is a parallelepiped meshed in elementary cubes, called voxels, whose size is determined by the user. Each voxel is either a fluid element, or a solid element depending on its occupation of solid. Thus, the complexity of the 3D geometry can be represented. In the computation, the Navier–Stokes–Brinkman equations are resolved (Wiegmann *et al.* 2009). The Brownian motion is considered with the Stokes–Einstein model. In case of collision particle – membrane surface, there is a capture condition mainly described by the Hamaker constant, the attractive energy of the particle. In case of bounce, the restitution coefficient represents the rate of recovered energy. In the present case, the electrostatic interactions have been neglected because the particle size is bigger than 0.7 μm. This geometry contains the following boundary conditions:

– In one direction, there are the inlet and the outlet.
– In the two other directions, there are periodic conditions.

A simulation contains several batches, of which the number of sent particles and the mean flux are fixed (here, 10^{-2} m s^{-1}). All the simulations have been realised with a monodisperse particle distribution. During a batch, all the particles start on the inlet surface. The position of the particles on the surface is determined randomly with a seed. Thus, with a same seed, the position of the particles is identical.

Modelling of the membrane

The used membrane is a 5 μm membrane produced by Millipore©. An X-ray tomography of the membrane provides a 3D image which can be imported in GeoDict. Thus, the resolution of the X-ray tomography determines the voxel size. In the present case, the voxel size is equal to 0.25 μm. The different macroscopic characteristics of these two membranes are presented in the Table 2. The good agreement between these values validates the representation of the membrane by GeoDict.

The X-ray tomography results yield also the pore size distribution (Figure 2). This distribution was obtained by numbering the opening on the membrane surface per size classes. The mean opening diameter is 2.41 μm. This value is half of the announced pore size (5 μm).

The geometry used in the simulations is presented Figure 3(a). It contains a void space thick of 200 voxels at

Table 2 | Macroscopic characteristics of the real and modelled membrane

	Real membrane	Modelled membrane
Thickness (μm)	135	135
Porosity	84%	83%
Permeability (m^2)	1.45×10^{-13}	1.33×10^{-13}

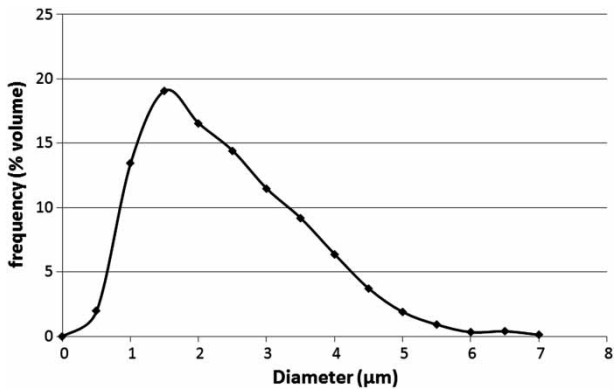

Figure 2 | Pore size distribution.

the inlet and a second void space of 50 voxels at the outlet. Thus, the inlet section is equal to 630 μm^2.

Simulation of particle capture

The simulation allows determining the position of the captured particles (Figure 3(b)). Nine particle diameters have been tested: from 0.7 to 6 μm. The voxel size of 0.25 μm limits the use of smaller particles. The Hamaker constant and the restitution coefficient were respectively set to 0 J and 1 in order to avoid physico-chemical capture and only have mechanical capture. Therefore, the results do not depend on the velocity. For each simulation, a constant volume of particles was sent. This volume is equal to 5% of the void volume of the membrane, which corresponds to 7.2 10^4 μm^3. Once the different batches done, the permeability of the final structure is computed. The capture efficiency is also obtained.

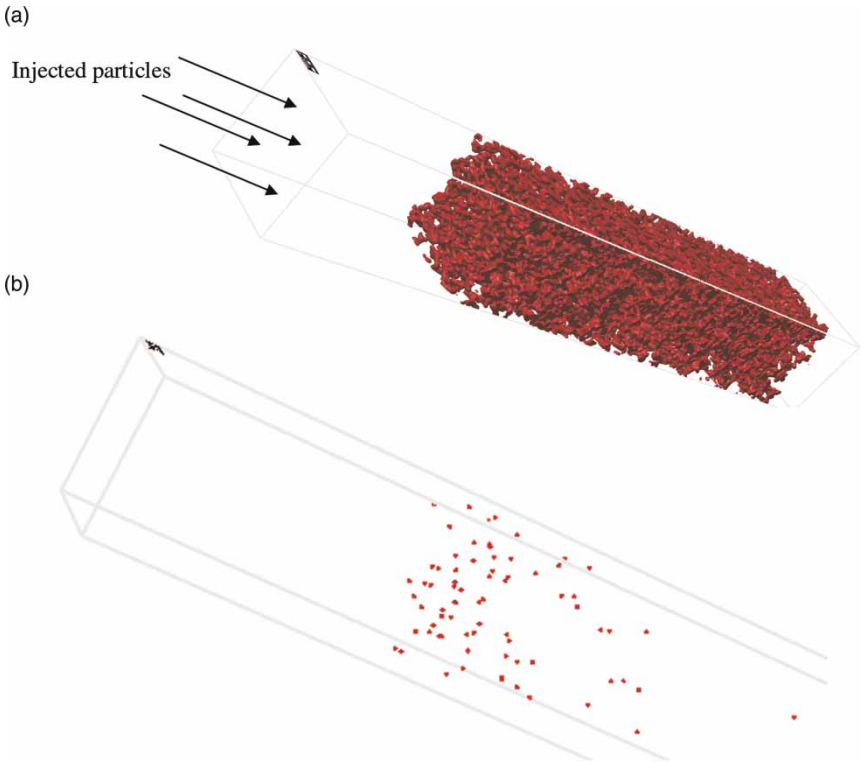

Figure 3 | (a) On the top, structure used for the simulation. Dimension: 100 × 745 × 101 voxels (25 × 186.25 × 27.5 μm). (b) On the bottom, position of the captured particles for a filtration of 0.7 μm particles. Here, the structure is hidden.

Table 3 | Fouling laws for each mechanism

Fouling mechanisms	$\Delta P = f(V_f)$	$L_p = f(M_p)$	
Complete pore blocking	$\frac{\Delta P_0}{\Delta P} = 1 - \frac{K_c V_f}{S J_0}$	$\frac{Lp}{Lp_0} = 1 - \frac{K_c M_p}{C_0 J_0}$	(2)
Standard pore blocking	$\frac{\Delta P_0}{\Delta P} = \left(1 - \frac{K_s}{2} V_f\right)^2$	$\frac{Lp}{Lp_0} = \left(1 - \frac{K_s S}{2C_0} M_p\right)^2$	(3)
Intermediate pore blocking	$\ln\left(\frac{\Delta P_0}{\Delta P}\right) = -K_i V_f$	$\ln\left(\frac{Lp}{Lp_0}\right) = -\frac{K_i S M_p}{C_0}$	(4)
Cake filtration	$\frac{\Delta P_0}{\Delta P} = \frac{1}{1 + K_g J_0 S V_f}$	$\frac{Lp}{Lp_0} = \frac{C_0}{C_0 + K_g J_0 S^2 M_p}$	(5)

Development of pore blocking law

The general law for dead-end filtration at constant flux (Equation (1)) can be decomposed for each fouling mechanism. These expressions are detailed in the Table 3, where the pressure drop through the membrane, ΔP, is given as a function of the filtered volume, V_f (first column), with K, a constant specific for each mechanism, S, the membrane section, J_0, the mean flux and C_0, the concentration of particles.

In the present case, it is easier to work with the permeability ratio and the mass of captured particles per square meter M_p. So, the relations were reformulated in this aim (second column of Table 3). The density of latex particles (1,050 kg m^{-3}) has been used for the simulations.

RESULTS AND DISCUSSION

Variation of the permeability

For each particle size, a same volume of particles has been sent. To avoid an overload of the inlet section, the total number of sent particles can be separated in several batches. The Table 4 presents the number of sent particles and the number of batches.

The curves of the filtration efficiency and of the ratio of the final permeability over the initial permeability are shown on the Figure 4.

For a particle diameter bigger than 1.25 μm, the results show that the fouling decreases with an increase of the particle size. Indeed, the particles become bigger than the pore size and are captured on the surface and put up a lower resistance to the flow. It is especially the case for the 4, 5 and 6 μm particles. So, more particles with a diameter higher than 4 μm must be sent to see an effect on the permeability of the simulated membrane ($A \approx 630\ \mu m^2$). Then, a minimum appears between 1 and 1.25 μm. This particle diameter is then slightly smaller than the pore size and about the cut-threshold. The presence of this minimum may be due to a change of fouling mechanism.

In order to better understand the causes, it is interesting to analyze the distribution of the captured particles in the depth of the membrane. On the Figure 5, the Cumulative Distribution Function (CDF) is represented over the relative depth, d^*.

$$d^* = \frac{2d}{e} \tag{6}$$

In this expression, d is the depth of the captured particle and e is the thickness of the membrane. So, if d^* is equal to 0, the particle is on the membrane surface and if d^* is equal to 1, the particle is in the middle of the membrane.

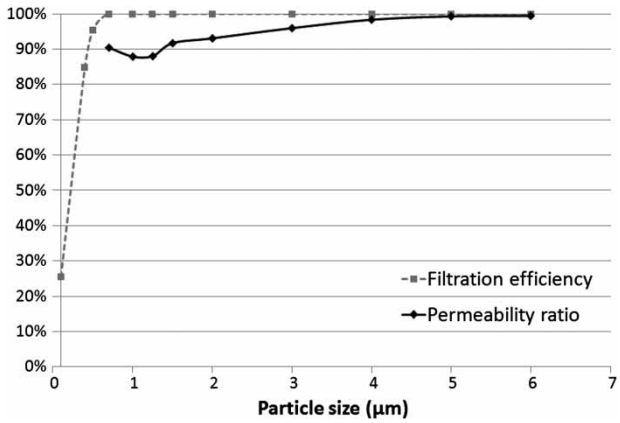

Figure 4 | Filtration efficiency and permeability ratio versus particle size for a same filtered volume.

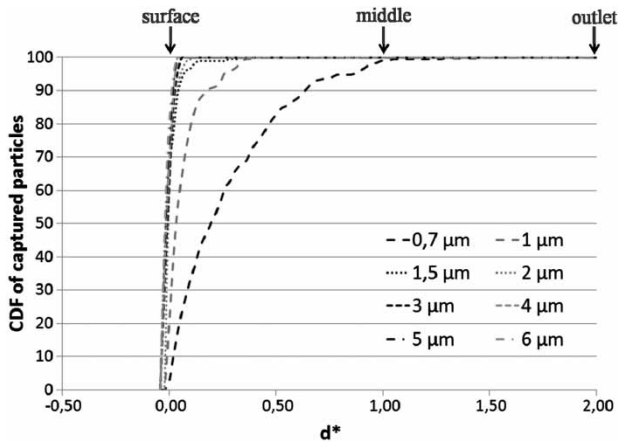

Figure 5 | Cumulative distribution function (CDF) of the captured particles versus d^*.

Table 4 | Number of sent particles and of batches for each size

Particles diameter (μm)	0.7	1	1.25	1.5	2	3	4	5	6
Sent particles	3,694	1,265	649	376	159	47	20	10	6
Number of batches	50	25	11	8	3	2	1	1	1

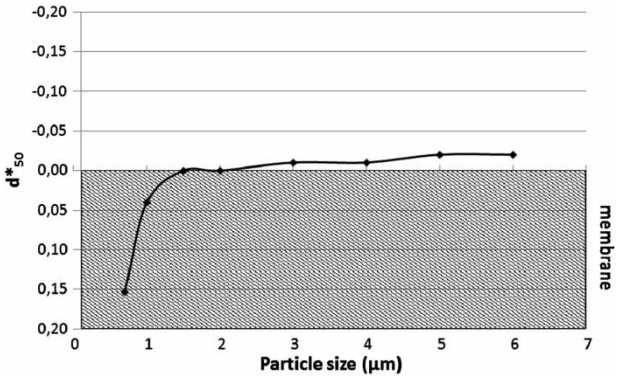

Figure 6 | d^* at 50% of the CDF versus particle size.

The particles with a size bigger than 1.5 µm do not penetrate in the membrane and stay on the surface. So, only intermediate and complete pore blocking can appear. For smaller particles, there is a real penetration. The Figure 6 plotting the relative depth, d^*, at 50% as a function of the particle size can confirm this view.

For the biggest particles, the d^*_{50} is negative. Therefore, the capture takes place on the surface and not in the pore, where the channels are reduced.

Evolution during filtered volume

Now, the study aims to determinate the predominant mechanism or the succession of predominant mechanisms. Because of the accuracy and the limited number of measures, the calculation of the first derivative of ΔP (Equation (1)) cannot be obtained cleanly. So the relations presented in the Table 3 were used. The Figure 7 shows the evolution of the permeability ratio during the filtered mass of particle per square meter for only three particle sizes: 0.7, 1 and 1.5 µm. With bigger particles, not enough particles have been sent and the variation of permeability is too low.

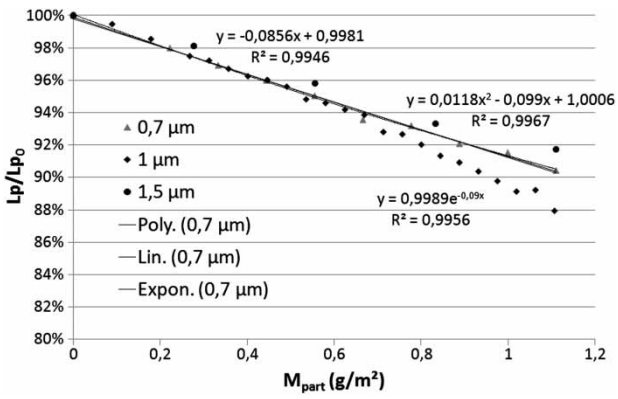

Figure 7 | Permeability ratio over the filtered mass per square meter.

Although the different curves seem to be some straight line (Equation (2)) (complete pore blocking mechanism), especially for the particle size of 0.7 and 1.5 µm, it is possible to liken these curves to the relations (Equation (3)) (standard pore blocking mechanism) or (Equation (4)) (intermediate pore blocking mechanism). All the fitting curves are mixed up, then, the predominant fouling mechanisms are still undetermined. However, a local approach can supply interesting data: the flow field and the pressure field. An increase of the pressure drop or of the velocity at a point may lead to a quantification of the fouling effect and, then, to the determination of a predominant fouling mechanism.

CONCLUSION

The membrane has been modelled thanks to an X-ray tomography measure and the macroscopic characteristics have been well represented. Based on this model, the simulations have highlighted the influence of the particle size on the permeability drop. The 1 µm particles cause the strongest fouling. This size is smaller than the mean pore size and slightly bigger than the cut-threshold. The position of the captures shows a penetration of the particles in the membrane for a diameter smaller than 1.5 µm. So a real penetration occurs for a particle size about half of the mean pore size. An analysis of the permeability evolution with the Hermia laws does not lead to the determination of the predominant fouling mechanism. Nevertheless, the microscopic scale approach supplies local data of velocity and of pressure. This information can quantify the fouling effects: increase of pressure drop and of velocity at some points. Then, that may lead to a more accurate analysis of the fouling mechanisms. Furthermore, the surface interactions are implemented in the model and also can be introduced. Some experiments are in progress to validate these numerical results.

REFERENCES

Bowen, W. R., Calvo, J. I. & Hernandez, A. 1995 Steps of membrane blocking in flux decline during protein microfiltration. *J. Membrane Sci.* **101** (1–2), 153–165.

Frey, J. M. & Schmitz, P. 2000 Particle transport and capture at the membrane surface in cross-flow microfiltration. *Chem. Eng. Sci.* **55** (19), 4053–4065.

Gonsalves, V. E. 1950 A critical investigation on the viscose filtration process. *Rec. Trav. Chim. Pays-Bas* **69**, 873.

Grace, H. P. 1956 Structure and performance of filter media. II. Performance of filter media in liquid service. *AIChE* **2** (3), 316–336.

Hermans, P. H. & Bredée, H. L. 1936 Principles of the mathematic treatment of constant-pressure filtration. *J. Soc. Chem. Ind.* **55T**, 1.

Hermia, J. 1982 Constant pressure blocking filtration laws–application to power law non-Newtonian fluid, Trans. *Inst. Chem. Eng.* **60** (3), 183–187.

Hwang, K.-J., Liao, C.-Y. & Tung, K.-L. 2008 Effect of membrane pore size on the particle fouling in membrane filtration. *Desalination* **234** (1–3), 16–23.

Kawakatsu, T., Nakajima, M., Nakao, S. & Kimura, S. 1995 Three-dimensional simulation of random packing and pore blocking phenomena during microfiltration. *Desalination* **101** (3), 203–209.

Seminario, L., Rozas, R., Borquez, R. & Toledo, P. G. 2002 Pore blocking and permeability reduction in cross-flow microfiltration. *J. Membrane Sci.* **209** (1), 121–142.

Wang, F. & Tarabara, V. V. 2008 Pore blocking mechanisms during early stages of membrane fouling by colloids. *J. Colloid Interface Sci.* **328** (2), 464–469.

Wiegmann, A., Rief, S., Latz, A. & Iliev, O. 2009 Toward predicting filtration and separation: Progress & Challenges, Filtech, 2009, pI-48-63.

First received 28 June 2010; accepted in revised form 2 September 2010